



**HAL**  
open science

## Experimental and modeling study of the oxidation of fenchone, a high-energy density fuel-additive

L. Boualem, Z. Serinyel, A. Nicolle, M. Lailliau, P. Dagaut, G. Dayma

### ► To cite this version:

L. Boualem, Z. Serinyel, A. Nicolle, M. Lailliau, P. Dagaut, et al.. Experimental and modeling study of the oxidation of fenchone, a high-energy density fuel-additive. *Fuel*, 2023, 353, pp.129183. 10.1016/j.fuel.2023.129183 . hal-04164151

**HAL Id: hal-04164151**

**<https://hal.science/hal-04164151>**

Submitted on 19 Jul 2023

**HAL** is a multi-disciplinary open access archive for the deposit and dissemination of scientific research documents, whether they are published or not. The documents may come from teaching and research institutions in France or abroad, or from public or private research centers.

L'archive ouverte pluridisciplinaire **HAL**, est destinée au dépôt et à la diffusion de documents scientifiques de niveau recherche, publiés ou non, émanant des établissements d'enseignement et de recherche français ou étrangers, des laboratoires publics ou privés.

Copyright

1                   **EXPERIMENTAL AND MODELING STUDY OF THE**  
2                   **OXIDATION OF FENCHONE, A HIGH-ENERGY DENSITY**  
3                   **FUEL-ADDITIVE**

4  
5                   **L. Boualem\*\*\*, Z. Serinyel\*\*, A. Nicolle\*\*\*, M. Lailliau\*\*, P. Dagaut\*\* and G.**

6                   **Dayma\*\*,\*\***

7                   guillaume.dayma@cnsr-orleans.fr

8                   \*Université d'Orléans, Château de la Source, avenue du Parc Floral, 45067 Orléans, France

9                   \*\*ICARE–CNRS, 1c avenue de la recherche scientifique, 45071 Orléans, France

10                  \*\*\*Aramco Fuel Research Center, 232 avenue Napoleon Bonaparte, 92852 Rueil-Malmaison, France

11  
12  
13                  **Abstract**

14                  Increasing fuel energy density constitutes a potential way to reduce engine exhaust carbon  
15                  emission. Fenchone, a strained ring molecule, could be an interesting candidate. The present  
16                  study investigates the oxidation of fenchone in a jet-stirred reactor at high pressure (10 atm)  
17                  between 700 and 1180 K at constant fuel mole fraction and constant residence time of 0.1%  
18                  and 0.7 s, respectively. Mole fraction profiles were obtained through sonic probe sampling, and  
19                  analyzed by gas chromatography and Fourier transform infrared spectrometry. More than 30  
20                  species were identified and most of them were quantified. Also, a kinetic mechanism is  
21                  developed in this study and tested against the present conditions showing good agreement. The  
22                  present mechanism allows to illuminate the major reaction pathways involved in the  
23                  decomposition routes of the fuel and its primary radicals as well as the formation pathways of  
24                  the quantified intermediate species. During fenchone oxidation, the carbonyl group is mostly  
25                  found in CO, CO<sub>2</sub> and formaldehyde while heavier carbonyl species were identified at much  
26                  lower quantities, indicating decarbonylation occurs early during the oxidation process.

27 Aromatic compounds such as benzene and toluene are formed especially in rich conditions  
28 while some potential oxygenated pollutants like methacrolein and acetaldehyde were quantified  
29 as well.

30

31

## 32 **1. Introduction**

33 Reformulation of transportation fuels through the incorporation of low-carbon blendstocks such  
34 as electrofuels constitutes an important option to address the pressing climate challenges [1].

35 The potential use of blendstocks and additives requires an in-depth knowledge of the  
36 combustion kinetics of the emerging components as well as of the nature and quantity of  
37 pollutants formed during their oxidation and thermal decomposition.

38 Strained ring hydrocarbons (SRH) are of interest as high-energy density components in  
39 transportation systems. These are readily produced from renewable feedstocks [2]. However,  
40 the impact of SRH on soot characteristics remains unclear [3], the respective importance of  
41 cyclopentadiene, fulvene and other benzene production routes being strongly dependent on  
42 combustion conditions [4]. Abdrabou et al. [5] showed that norbornane addition to a Diesel fuel  
43 involves a threshold soot index reduction and soot disorder increase, as a result of five-  
44 membered ring incorporation in the molecular structure of soot [6, 7]. Functionalizing SRH  
45 with oxygen-containing groups, such as alcohols or ketones, may help in further reducing SRH  
46 sooting propensity [8], however at the expense of the SRH calorific value. In a recent study by  
47 Morajkar et al. [9], the effect of the addition of solid camphor and camphor oil to Diesel fuel  
48 on its sooting propensity is studied using a diffusion flame. The authors reported  
49 physicochemical changes such as a smaller particle diameter in the presence of camphor, which  
50 they linked to the increased oxidative reactivity.

51

52 Combustion characteristics of the SRH is insufficiently addressed. Among these  
53 hydrocarbons, JP-10 (mostly endo-tetrahydrodicyclopentadiene), produced by the catalytic  
54 hydrogenation of dicyclopentadiene, is probably the most studied one; e.g. [4, 10-12]. The aim  
55 of the present work is to study experimentally the combustion mechanism of fenchone (1,3,3-  
56 trimethyl-bicycloheptan-2-one), a monoterpenoid present in fennel oil, and to provide a  
57 predictive pollutant formation model in oxygenated SRH combustion, opening up the use of  
58 such SRH for specific transport applications. Table 1 presents a comparison between octane  
59 number (RON, MON), lower heating value (LHV), and boiling point for fenchone and few  
60 other popular additives.

61 Fenchone can be found in wormwood with a concentration lower than  $5 \text{ mg L}^{-1}$ . It can also  
62 be found in essential oils extracted from fennel seeds in varying concentrations depending on  
63 the species of fennel and its growing place. According to the European Pharmacopoeia, the  
64 essential oil of bitter fennel produced from the aerial parts of the plant (*Foeniculum Vulgare*)  
65 may contain between 7 and 25% of fenchone. This monoterpene is used as a raw material for  
66 the manufacture of flavours in food and perfumery. It can also be used in beverages as a  
67 preservative or in detergents and soaps.

68 The only combustion-related study on fenchone goes back to 2014, which reports the  
69 laminar flame speeds of fenchone at 453 K [13]. Their results suggest that the laminar flame  
70 speeds of fenchone are close to those of JP-10 previously measured by Parsinejad et al. [12],  
71 on the lean side and very close to those of  $\alpha$ -pinene [14]. To the best of our knowledge, except  
72 flash pyrolysis experiments performed in the 1960's [15], there are no oxidation or pyrolysis  
73 studies reporting intermediate species, hence providing details on fenchone decomposition  
74 routes.

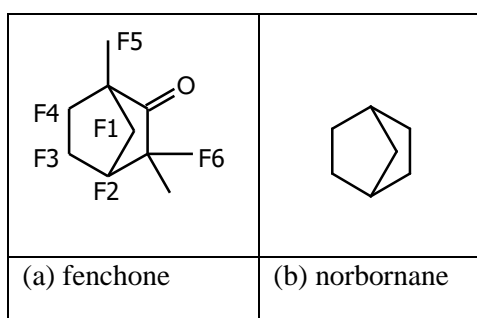
75 Table 1: Main characteristics of some popular additives.

Compound	RON [16]	MON [16]	LHV (MJ/kg) [17]	BP (°C)
fenchone	93	81	38	192
diisopropylketone	102	93	36	125
2-butanone	109	104	32	80
isobutanol	103	91	33	108
cyclopentanone	103	90	32	131

76

77 The molecular structure of fenchone is illustrated in Figure 1. Among the high-density  
78 hydrocarbon fuels, structural similarities can be drawn between fenchone and norbornane (as  
79 well as 2-ethylnorbornane) for which limited theoretical studies exist. For example, recently  
80 Wang et al. [18] calculated the bond energies of 2-ethylnorbornane, norbornadiene and  
81 quadricyclane at the CCSD(T)/cc-PVTZ//B3LYP/6-311++g(d,p) level of theory. According to  
82 their calculations and based on similarities, F2 (see Fig. 1 for radicals' names) is the least likely  
83 radical to be formed with a C–H bond energy around 107 kcal mol<sup>-1</sup> followed by F1 with 104–  
84 105 kcal mol<sup>-1</sup>. On the other hand, C–H bonds at positions F5–F6 (101.4 kcal mol<sup>-1</sup>) and F3–  
85 F4 (98.7 kcal mol<sup>-1</sup>) are quite similar to primary (~101 kcal mol<sup>-1</sup>) and secondary (~98.5 kcal  
86 mol<sup>-1</sup>) C–H bond energies in alkanes.

87



88 **Figure 1.** Structure of fenchone (a), and norbornane (b). Fx denotes the name of the radical in  
89 the mechanism according to the position of the free electron.

90

91 Sirjean et al. [19] used ab initio methods to calculate some important reaction rate constants  
92 in the decomposition of norbornane, at the CBS-QB3 level of theory. In Sirjean et al. [19], the  
93 spin-contamination energy correction which they proposed pertains to biradicals which are not  
94 considered in the present study. No symmetry correction to CBS-QB3 values were necessary  
95 either as the structures considered are not symmetric, unlike some species featured in Sirjean's  
96 study. The lowest energy conformer obtained by MMFF94 optimization was used as a guess  
97 for CBS-QB3 calculations within the RRHO approximation. As radical formation enthalpies  
98 are deduced from reference (fenchone) value and difference of CBS-QB3 enthalpies, the  
99 remaining errors (estimated to be lower than 2 kcal mol<sup>-1</sup>) should partially cancel out between  
100 the structures calculated. Regarding isodesmic reactions, fenchone standard formation enthalpy  
101 was calculated using the following reaction: fenchone + 3 propane  $\rightleftharpoons$  norbornane + acetone +  
102 neopentane + isobutane. Given that there are no theoretical studies in the literature on fenchone  
103 oxidation and ab initio rate constant calculation was outside of the scope of the present study,  
104 structure/reactivity analogies were made for the mechanism development (see section 3).

105

106 In the present study, oxidation experiments of dilute fenchone/O<sub>2</sub>/N<sub>2</sub> mixtures were carried  
107 out in a jet-stirred reactor at equivalence ratios of 0.5–2 and at 10 atm, between 700–1180 K,  
108 with 1000 ppm as an initial mole fraction of fenchone. Reactants, products and intermediate  
109 species were measured and quantified. A kinetic mechanism is developed in order to understand  
110 the oxidation pathways of fenchone.

111

## 112 **2. Experimental set-up**

113 The present experiments were performed in a jet-stirred reactor, described in detail elsewhere.

114 The reactor used for this study has been described by Dagaut et al. [20]. It is a 4 cm diameter

115 fused-silica sphere (42 cm<sup>3</sup>) with four injectors (nozzles of 1 mm I.D). This apparatus has been

116 designed to provide stirring under the present conditions. An HPLC pump (LC10 AD VP) with  
117 an online degasser (Shimadzu DGU-20 A3) was used to inject 1000 ppm of fenchone (>99%  
118 pure from Aldrich, L-fenchone was used) into the reactor. The fuel is pushed towards the  
119 reaction sphere with an auxiliary N<sub>2</sub> flow and meets the O<sub>2</sub>/N<sub>2</sub> primary flows just before the  
120 JSR injectors to avoid premature fuel oxidation. The gas flow rates were controlled by mass  
121 flow controllers (Brooks). The whole assembly is maintained at a temperature higher than the  
122 boiling point of the fuel (467 K) to facilitate the fuel evaporation. A probe coupled with a  
123 thermocouple (0.1 mm Pt-Pt/Rh-10%), inserted into a thin-walled fused silica tube to avoid any  
124 catalytic reactions on the metallic wires, allows the sampling at each desired temperature. To  
125 ensure the homogeneity of the mixture, the probe can be moved along the vertical axis of the  
126 reactor and the temperature gradient was measured to be less than 2 K cm<sup>-1</sup>.

127

128 At each selected temperature point, the reaction mixture was sampled using a low-pressure  
129 fused silica sonic probe. The samples were sent to the analysers through a heated Teflon line  
130 maintained at 160°C. These samples are analysed using a Thermo Nexus 670 spectrometer (10  
131 m path length, resolution 0.5 cm<sup>-1</sup>, 200 mbar in the cell). The gas samples can also be stored at  
132 low-pressure in Pyrex bulbs for off-line gas chromatography analysis. Two types of detector  
133 were used. A TCD detector coupled to a CP-Carboplot-P7 capillary column allows the  
134 quantification of O<sub>2</sub>. A FID detector using a CP-Al<sub>2</sub>O<sub>3</sub>-KCl column in a Shimadzu GC-MS  
135 2010 Plus and a CP-SIL 5CB coupled to DB1 column was used to measure hydrocarbons and  
136 oxygenated compounds. Both chromatographs are coupled with a mass spectrometer operating  
137 with electron impact ionization (70 eV) for product identification. The different acronyms are  
138 listed in Table 2.

139 Table 2: List of acronyms.

FID	Flame Ionization Detector
GC-MS	Gas Chromatography- <u>Mass Spectrometry</u>

TCD	Thermal conductivity detector
FTIR	Fourier-Transform Infrared Spectrometry
HPLC	High-Pressure Liquid Chromatography
CP-SIL	ChromPack-DimethylpolySiloxane Column
CP-Al <sub>2</sub> O <sub>3</sub> -KCl	ChromPack Aluminium Oxide Column deactivated by Potassium Chloride
CP-Carboplot-P7	ChromPack Carbon-Based Porous Layer Open Tubular Column

140

141 The species quantified in this study are final products and stable intermediates such as H<sub>2</sub>,  
142 CH<sub>4</sub>, C<sub>2</sub>H<sub>4</sub>, C<sub>2</sub>H<sub>6</sub>, C<sub>3</sub>H<sub>6</sub>, allene, propyne, isoprene, methyl cyclopentadienes, benzene, or  
143 toluene were measured by gas chromatography. Few other oxygenated species were also  
144 quantified including fenchone, acetone, acetaldehyde, acrolein, methacrolein, and methyl vinyl  
145 ketone. H<sub>2</sub>O, CO, CO<sub>2</sub>, CH<sub>2</sub>O were measured by online FTIR. The carbon balance was checked  
146 for each sample and found to be within  $\pm 15\%$ . The uncertainty on reactants and N<sub>2</sub> flow rates  
147 was  $< 5\%$ , which has an impact on the residence time and the measured mole fractions [21, 22].  
148 Several heavier hydrocarbons, with one or more double bonds, were separated by GC but their  
149 identification was not possible. According to their global formulae, using the equivalent carbon  
150 method, their mole fractions were typically  $< 10$  ppm.

151

### 152 **3. Kinetic mechanism**

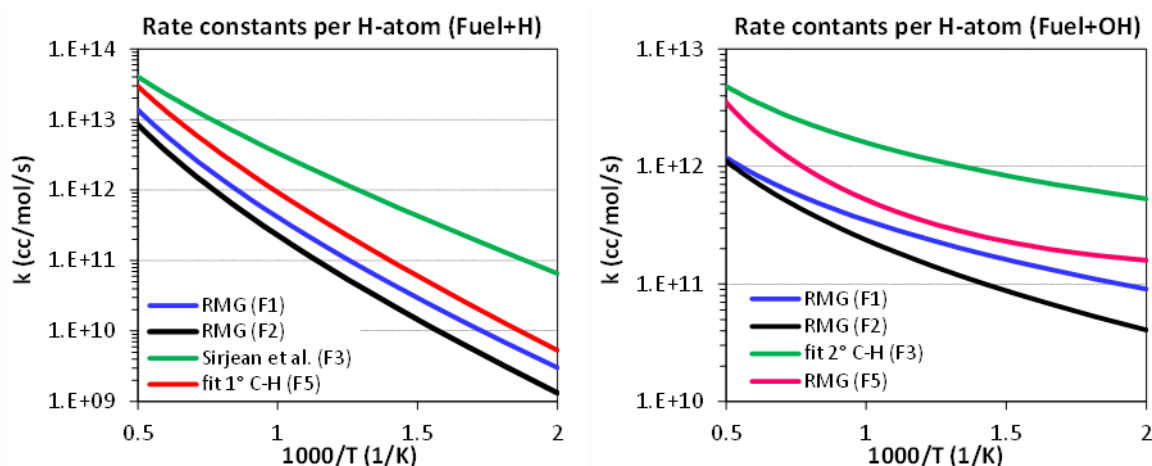
153 The kinetic sub-mechanism of fenchone, a summary of the most important reactions of which  
154 is presented in SM1, was developed and integrated into our C<sub>5</sub> mechanism [23]. We have  
155 considered the formation of all six possible radicals even though F1 and F2 are very unlikely  
156 to be formed under our operating conditions due to higher BDEs [18]. This sub-mechanism was  
157 mostly developed following the commonly accepted reaction classes, and the RMG website  
158 [24] was used in order to evaluate some rate constants and thermochemistry. As a first and  
159 simplified approach, F3 and F4 were considered as equivalent, contrary to F1, and are thus

160 supposed to be formed at the same rate. Similarly, F5 and F6 were also both considered as  
161 equivalent, F6 being formed twice as much as F5 because of the number of available H atoms.  
162

163 Unimolecular initiation reactions by C–H bond breaking were taken from RMG website  
164 considering a pressure dependency (rates at 10 atm were considered in this work). Bimolecular  
165 initiation steps were also considered and taken from RMG. The formation of biradicals was  
166 found to be negligible under our conditions and thus not included.

167  
168 For hydrogen abstraction reactions by H atoms, presented in Figure 2 (left), and CH<sub>3</sub>  
169 radicals, the rate constants calculated by Sirjean et al. (for norbornane) [19] were used as best  
170 analogy for the formation of radicals F3 and F4. For radicals F5 and F6, analogies with respect  
171 to similar sites in alkanes were considered. For F1 and F2, rate constants proposed on the RMG  
172 website were kept.

173



174

175 **Figure 2.** Rate constants for H-abstraction reactions by H (left) and OH (right). F3 and F4 are  
176 supposed to have the same rate constants while F6 has twice that of F5.

177

178 For H-abstraction reactions by OH radicals, also shown on Figure 2 (right), rate constants  
179 suggested by RMG were chosen except for the F3 and F4 radicals (with bond energies similar

180 as a secondary C–H site in an alkane) where RMG generated rate constants were the same as  
181 that for F1 radical. For these secondary C–H sites, rate constants used for alkanes were  
182 preferred. These rate constants referred to as ‘fit’ in the legend of Figure 2 are typical rate  
183 constants that can be used for alkanes for H-abstraction reactions. These are obtained by  
184 considering several rate constants from the literature (references to these rate constants and the  
185 fits for each C–H site can be found in the supplementary material) and fitting them over a wide  
186 temperature range.

187

188 Rate constants of the beta-scission and internal H-transfer reactions of the fuel radicals,  
189 were evaluated through RMG website [24]. Once the 6 primary radicals (F1 to F6) are  
190 decomposed, the rate constants of the reactions involved in the consumption/formation of the  
191 subsequent species were also taken from RMG website with no modifications. The reaction of  
192 resonantly stabilized radicals with HO<sub>2</sub>, yielding an aldehyde (or a ketone) and a smaller radical,  
193 was considered with a rate constant of  $4.50 \times 10^{12} \text{ mol cm}^{-3} \text{ s}^{-1}$ .

194

195 Thermochemical properties of all species included into our mechanism were evaluated  
196 through group additivity method implemented in RMG [22] as well. However, it was necessary  
197 to revise the estimated thermochemistry for radicals F1, F2, and F3 considering the differences  
198 observed on bond dissociation energies with what was expected (see Introduction). Ab initio  
199 electronic structure calculations at the CBS-QB3 level of theory implemented in Gaussian 16  
200 [25] and isodesmic reactions were used to get more accurate results in terms of BDEs. The  
201 mechanism file, thermochemistry file, nomenclature and SMILES notations of these species  
202 are provided as supplementary material.

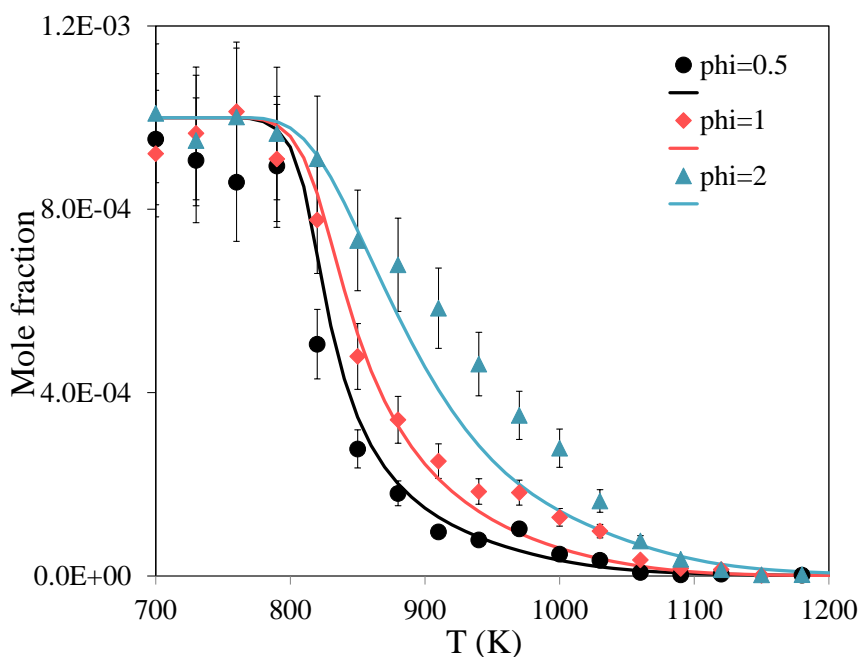
203

204 **4. Results and discussion**

205 The present section presents a wide range of experimental conditions performed at a constant  
206 mean residence time of 0.7s and a constant pressure of 10 atm. Three different equivalence  
207 ratios were investigated from fuel-lean to fuel-rich ( $\phi = 0.5, 1, 2$ ). The initial mole fraction of  
208 fenchone was set to 1000 ppm for the whole experiment, and the temperature ranged from 700  
209 to 1180 K.

210  
211 More than 30 species were detected including alkanes ( $C_1-C_3$ ), alkenes ( $C_2-C_5$ ), dienes ( $C_4-$   
212  $C_6$ ), cyclic olefins, aromatics, and oxygenated compounds. Figure 3 illustrates the evolution of  
213 the reactants as a function of the temperature where it can be observed that the reactivity starts  
214 just below 800 K independently of the equivalence ratio. Moreover, the fuel conversion for the  
215 fuel-lean mixture appears to be substantially higher than that of the fuel-rich mixture. The  
216 developed kinetic mechanism captures well the onset of the reactivity as well as the fuel  
217 consumption for the fuel-lean and the stoichiometric mixtures, but predicts a slightly excessive  
218 reactivity between 900-1050 K for the fuel-rich mixture.

219

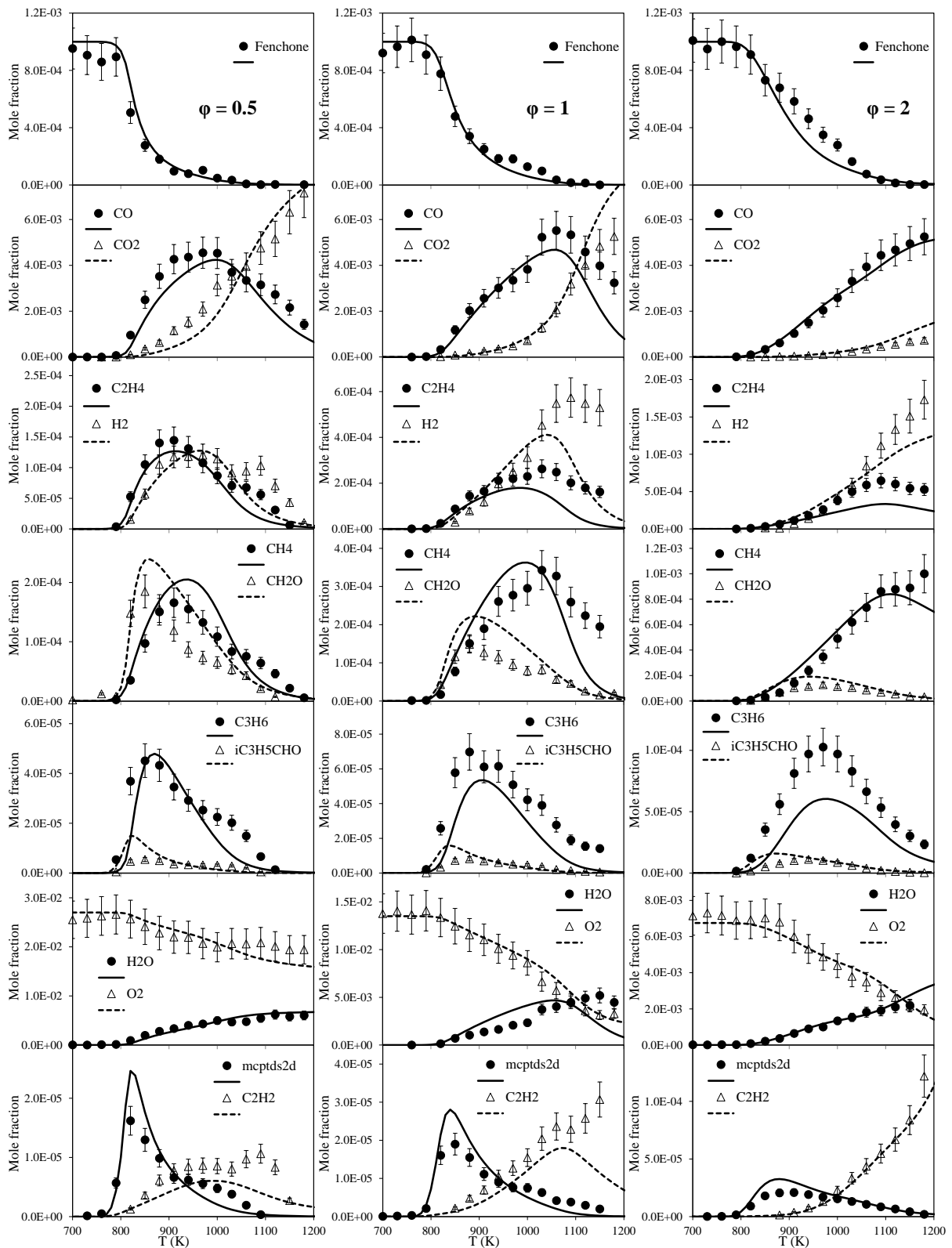


220

221 **Figure 3.** Evolution of the mole fractions of fenchone as a function of temperature for three  
222 different equivalence ratios at  $p = 10$  atm,  $\tau = 0.7$  s.

223

224 The evolution of the mole fractions of the reactants (Fenchone and  $O_2$ ), and major species  
225 are presented in Figure 4. The major intermediate species are  $CH_4$ ,  $C_2H_4$ , and  $CH_2O$  whose  
226 maximum mole fractions are 2000 ppm and 1750 ppm for  $CH_4$  and  $C_2H_4$  respectively for the  
227 rich mixture, whereas formaldehyde is in the order of 180 ppm for all mixtures. As expected,  
228 the concentrations of aromatic species increase with the equivalence ratio, the most abundant  
229 one being benzene. At  $\phi = 2$ , its mole fraction reaches almost 200 ppm, while it is only 20 ppm  
230 at  $\phi = 0,5$ . Toluene and xylene were also identified in comparable proportions, their mole  
231 fractions being the highest for the fuel-rich mixture. Less than 10 ppm of styrene were also  
232 detected at  $\phi = 2$  and trace amounts in the other conditions. Low quantities of several cyclic  
233 species were also observed, such as cyclopentadiene and two different methyl-cyclopentadiene  
234 which are formed with similar mole fractions. Finally, among the oxygenated intermediates,  
235 acetone, acrolein, methyl vinyl ketone, and methacrolein were also quantified, their mole  
236 fractions being higher under fuel-lean conditions.



237

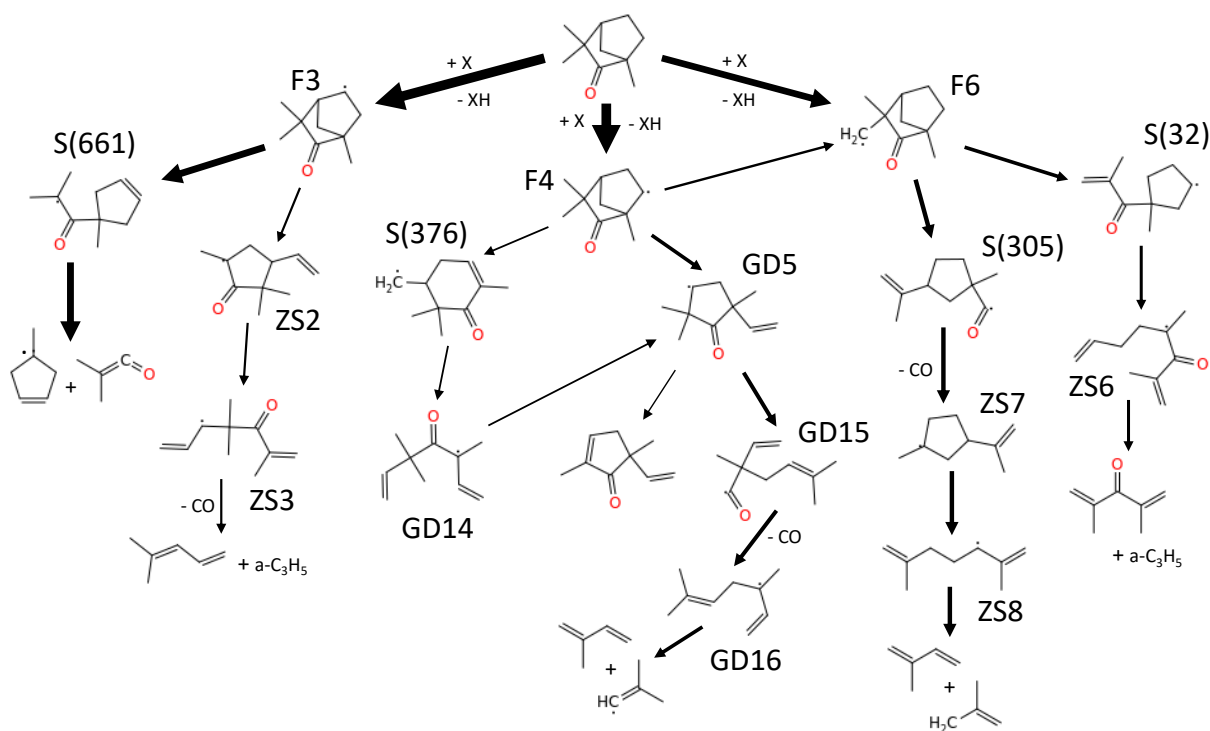
238 **Figure 4.** Evolution of the mole fractions of fenchone, O<sub>2</sub>, and several stable products as a

239 function of temperature for three different equivalence ratios at p = 10 atm, τ = 0.7 s.

240

241 As can be seen from Figure 4, the developed kinetic mechanism captures well the general  
 242 trend of the fuel consumption as well as the formation and consumption of the different  
 243 intermediates. Experimentally, it can also be observed that the reactivity slightly decreases (or,  
 244 at least, does not keep increasing with the temperature) over the temperature range 900-1050  
 245 K. This decrease is more and more pronounced when the equivalence ratio increases. It can  
 246 possibly be attributed to the accumulation of heavy stable intermediates which were not  
 247 experimentally detected. This decrease in reactivity is not really captured by the model and a  
 248 more accurate prediction of this phenomenon would constitute a significant improvement of  
 249 the understanding of the oxidation of fenchone at high temperature. Nevertheless, considering  
 250 the good agreement observed between calculations and experiments at lower temperature, a  
 251 reaction pathway analysis was performed under stoichiometric condition and  $T = 850$  K  
 252 (temperature at which half of the fenchone is consumed) to unravel the major consumption  
 253 routes of fenchone under these conditions. The result of this reaction pathways analysis is  
 254 presented in Figure 5.

255



256

257 **Figure 5.** Reaction pathways analysis for the oxidation of fenchone at  $\phi = 1$ ,  $p = 10$  atm,  $\tau =$   
258 0.7 s, and  $T = 850$  K. Arrow thickness denotes the intensity of respective carbon flux.

259

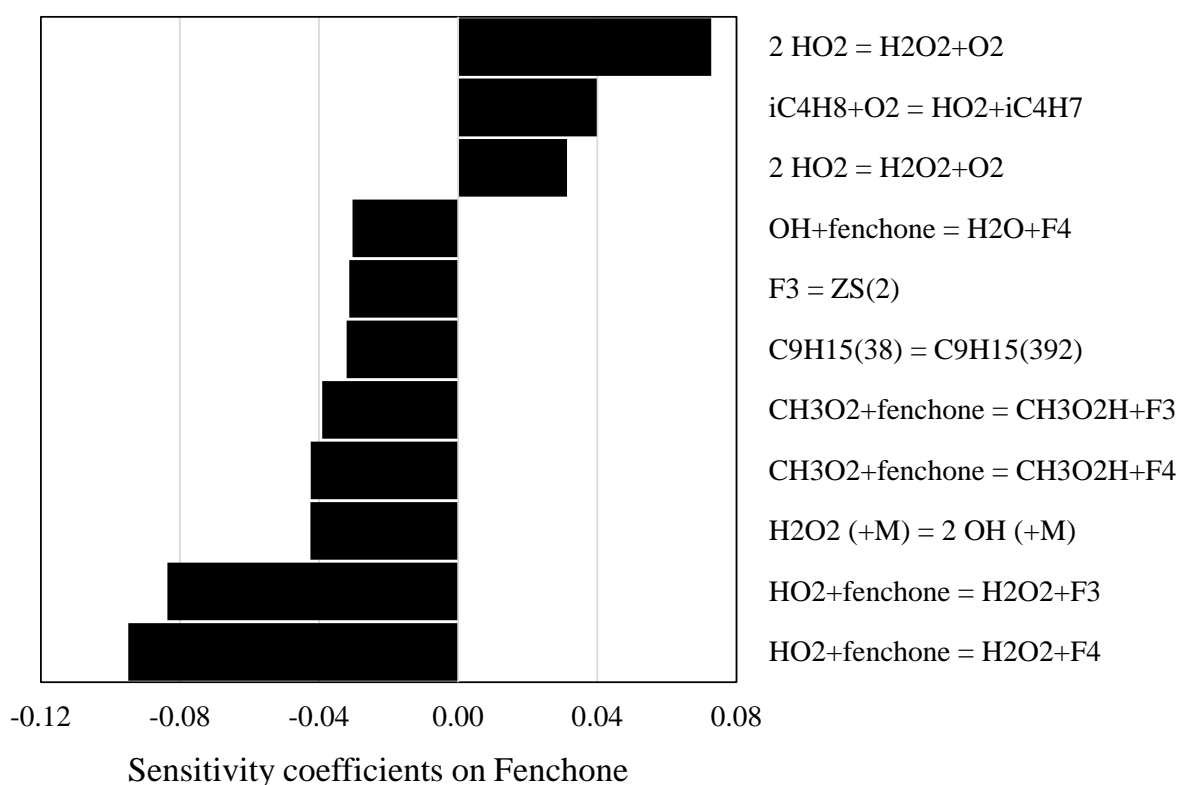
260 As illustrated by Figure 5, fenchone is mainly consumed by H-abstraction reactions by OH  
261 yielding F3 and F4 at the same rate. Though being less formed than the two previous, F6 is the  
262 third most important primary radical in this analysis, F5, F1, and F2 being almost negligible  
263 (9%, 5%, and 4% respectively). The fate of F3, F4, and F6 is discussed in the following:

264 F3- Almost three quarters of F3 decompose into 4-isobutenoxy-4-methyl-1-  
265 cyclopentene, S(661), which reacts completely to yield a methyl cyclopentenyl radical and  
266 opens the route to benzene, which will be elaborated in the next paragraph. The remaining  
267 quarter leads to allyl radical and methyl pentadiene which was not observed experimentally.  
268 The third possible C-C  $\beta$ -scission, opening the bridge over the six-membered ring and yielding  
269 a radical of a ramified cyclohexanone, appears to be negligible under these conditions.

270 F4- A quarter of F4 isomerizes into F6, while more than a third produces GD5  
271 (C=CC1(C)C[CH]C(C)(C)C(=O)1). The latter is also formed by cyclization of a radical  
272 obtained from the 6-membered ring opening. A quarter of GD5 yields a ramified  
273 cyclopentenone, the rest producing isoprene and the vinylic isobutenyl radical after ring  
274 opening and decarbonylation. This isobutenyl radical is mostly responsible for the formation of  
275 acetone. Two other C-C  $\beta$ -scission reactions were considered to consume F4, but it turns out  
276 that they are both negligible under these conditions.

277 F6- The two pathways consuming F6 are similar in terms of flow rate. One yields  
278 isoprene after decarbonylation and ring opening, whereas the other one produces diisopropenyl  
279 ketone, which was not observed experimentally. A third C-C  $\beta$ -scission was also considered for  
280 F6 producing  $\text{CH}_3$  radicals, but turns out to be negligible because of its high activation energy  
281 resulting from RMG rate rules.

282 In order to complete the picture we have of the reactivity of fenchone, a sensitivity analysis  
 283 on the fuel was carried out at 770 K for the stoichiometric mixture. As can be seen from Figure  
 284 6, under these conditions, fenchone consumption is mostly sensitive to H-abstraction reactions  
 285 by HO<sub>2</sub>, and CH<sub>3</sub>O<sub>2</sub> to a lesser extent, yielding radicals F3 and F4, i.e. the secondary radicals.  
 286 Therefore, fenchone is also sensitive to reactions producing or consuming HO<sub>2</sub> and H<sub>2</sub>O<sub>2</sub>. More  
 287 interestingly, fenchone oxidation is also sensitive to ring opening reactions such as F3 into ZS2  
 288 or C<sub>9</sub>H<sub>15</sub>(38) = C<sub>9</sub>H<sub>15</sub>(392) (see Fig. 5 and supplementary material for structures).

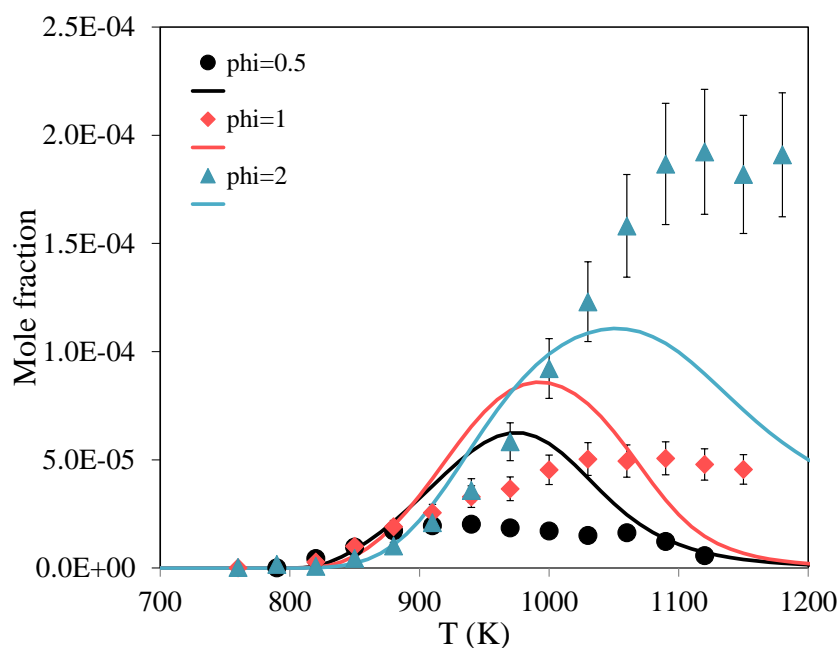


289  
 290 **Figure 6.** Sensitivity analysis on fenchone at  $\phi = 1$ ,  $p = 10$  atm,  $\tau = 0.7$  s, and  $T = 770$  K.

291  
 292 Benzene was produced in significant amounts during the oxidation of fenchone. Other  
 293 aromatic compounds such as toluene, styrene, xylenes, trimethyl benzenes or methyl styrene  
 294 were also observed especially under fuel-rich conditions. Unfortunately, our kinetic mechanism  
 295 is not developed to model the formation and consumption of aromatic species, and  
 296 improvements on the basis of the present results would be too limited. However, the particular

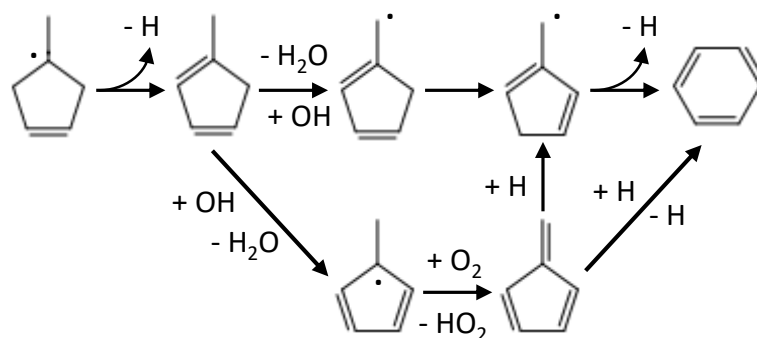
297 case of benzene represents a way of possible improvements to better understand the different  
 298 steps occurring during this process. Figure 7 illustrates how benzene is overestimated by the  
 299 model under fuel-lean conditions but under estimated at high temperature under fuel-rich  
 300 conditions. A reaction pathway analysis was performed at  $\phi = 1$  and  $T = 950$  K, revealing that  
 301 benzene is mostly produced by the reactions of methyl cyclopentenyl radicals, methyl  
 302 cyclopentadienes, methyl cyclopentadienyl radicals, and fulvene. This rate of production  
 303 analysis is presented in Figure 8 where it can be seen that benzene mostly comes from radical  
 304 F3 through the formation of methyl cyclopentenyl radicals. Our kinetic mechanism has been  
 305 significantly modified, in order to account for recent  $\text{CH}_3 + \text{C}_5\text{H}_5$  rate constant calculations by  
 306 Krashnoukov et al. [26], but efforts are still required to better represent benzene accumulation  
 307 under these conditions, given the diversity of  $\text{C}_6$  intermediates and the corresponding benzene  
 308 formation and consumption pathways [27].

309



310

311 **Figure 7.** Evolution of the mole fractions of benzene as a function of temperature for three  
 312 different equivalence ratios at  $p = 10$  atm,  $\tau = 0.7$  s.



313

314 **Figure 8.** Routes of formation of benzene at  $p = 10$  atm,  $\tau = 0.7$  s, and  $\phi = 1$ .

315

### 316 **Conclusions**

317

318 In the present study, we have investigated the oxidation chemistry of fenchone via detailed  
 319 speciation experiments in a jet-stirred reactor. Fenchone is a strained-ring hydrocarbon with  
 320 potentially interesting characteristics (e.g. high energy density) and as a high-octane component  
 321 however its oxidation chemistry has not been dissected before. A detailed kinetic sub-  
 322 mechanism of fenchone is also developed mostly using the RMG website and complementary  
 323 structure/reactivity relations with similar hydrocarbons when available. Three equivalence  
 324 ratios were chosen for the experiments in order to assess the differences in reactivity. In terms  
 325 of fuel conversion, the fuel-rich mixture was found to be the least reactive one, and is also the  
 326 one that produced more benzene. Reaction pathway analyses showed that benzene formation is  
 327 closely linked to the chemistry of methyl cyclopentenyl radicals, methyl cyclopentadiene  
 328 isomers, methyl cyclopentadienyl radicals, and fulvene. These could constitute future targets  
 329 for model improvement. Apart from benzene, toluene as well as traces of styrene were identified  
 330 as aromatic species. Among potential oxygenated pollutants, formation of acrolein and  
 331 methacrolein is observed. Overall, the kinetic mechanism showed good agreement with the  
 332 present experimental data and helped us identify the underlying reaction pathways. Further

333 perspectives could be the investigation of global combustion properties of fenchone in  
334 environments close to engine operation such as ignition delay times.

335

### 336 **Acknowledgement**

337 Support from the CAPRYSESSES project (ANR-11-LABX-006-01) funded by the PIA  
338 (Programme d'Investissement d'Avenir) is gratefully acknowledged. The authors thank  
339 Aramco Overseas Company for supporting this research.

340

### 341 **References**

342 [1] Ausfelder F, Wagemann K. Power-to-Fuels: E-Fuels as an Important Option for a  
343 Climate-Friendly Mobility of the Future. *Chem Ing Tech* 2020;92(1-2):21-30.

344 [2] Meylemans HA, Quintana RL, Harvey BG. Efficient conversion of pure and mixed  
345 terpene feedstocks to high density fuels. *Fuel* 2012;97(Supplement C):560-568.

346 [3] Zaabi AA, Raj A, Elkadi M, Anjum D, Li L, George A, Shebli MNA. Effects of the  
347 addition of a high energy density fuel, adamantane to diesel on its cetane number, sooting  
348 propensity, and soot nanostructural properties. *Cleaner Chemical Engineering*  
349 2022;2:100008.

350 [4] Vandewiele NM, Magoon GR, Van Geem KM, Reyniers M-F, Green WH, Marin GB.  
351 Kinetic Modeling of Jet Propellant-10 Pyrolysis. *Energy & Fuels* 2015;29(1):413-427.

352 [5] Abdrabou MK, Morajkar PP, Guerrero Peña GDJ, Raj A, Elkadi M, Salkar AV. Effect of  
353 5-membered bicyclic hydrocarbon additives on nanostructural disorder and oxidative  
354 reactivity of diffusion flame-generated diesel soot. *Fuel* 2020;275:117918.

355 [6] Salamanca M, Botero ML, Martin JW, Dreyer JAH, Akroyd J, Kraft M. The impact of  
356 cyclic fuels on the formation and structure of soot. *Combust Flame* 2020;219:1-12.

- 357 [7] Andrews RJ, Smith CF, Alexander AJ. Mechanism of carbon nanotube growth from  
358 camphor and camphor analogs by chemical vapor deposition. *Carbon* 2006;44(2):341-  
359 347.
- 360 [8] Barrientos EJ, Lapuerta M, Boehman AL. Group additivity in soot formation for the  
361 example of C-5 oxygenated hydrocarbon fuels. *Combust Flame* 2013;160(8):1484-1498.
- 362 [9] Morajkar PP, Guerrero Peña GDJ, Raj A, Elkadi M, Rahman RK, Salkar AV, Pillay A,  
363 Anjana T, Cha MS. Effects of Camphor Oil Addition to Diesel on the Nanostructures and  
364 Oxidative Reactivity of Combustion-Generated Soot. *Energy & Fuels* 2019;33(12):  
365 12852-12864.
- 366 [10] Gao CW, Vandeputte AG, Yee NW, Green WH, Bonomi RE, Magoon GR, Wong H-W,  
367 Oluwole OO, Lewis DK, Vandewiele NM, Van Geem KM. JP-10 combustion studied  
368 with shock tube experiments and modeled with automatic reaction mechanism  
369 generation. *Combust Flame* 2015;162(8):3115-3129.
- 370 [11] Zhong B-J., Zeng Z-M., Zhang H-Z. An experimental and kinetic modeling study of JP-  
371 10 combustion. *Fuel* 2022;312:122900.
- 372 [12] Parsinejad F, Arcari C, Metghalchi H. Flame Structure and Burning Speed of JP-10 Air  
373 Mixtures. *Combust Sci Technol* 2006;178(5):975-1000.
- 374 [13] Coudour B, Chetehouna K, Courty L, Garo JP, Lemée L, Mounaïm-Rousselle C, Halter  
375 F. Combustion Characteristics of Two Biogenic Volatile Organic Compounds: L-  
376 Fenchone and 3-Hexen-1-ol. *Combust Sci Technol* 2014;186(10-11):1284-1294.
- 377 [14] Courty L, Chetehouna K, Halter F, Foucher F, Garo JP, Mounaïm-Rousselle C.  
378 Experimental determination of emission and laminar burning speeds of  $\alpha$ -pinene.  
379 *Combust Flame* 2012;159(4):1385-1392.

- 380 [15] Sato T, Murata K, Nishimura A, Tsuchiya T, Wasada N. Pyrolysis of organic compounds-  
381 II: The flash pyrolysis of camphor and its related compounds. *Tetrahedron*  
382 1967;23(4):1791-1798.
- 383 [16] GNN, <https://gnn.avt.rwth-aachen.de> [accessed May 2023].
- 384 [17] Li R, Herreros JM, Tsolakis A, Yang W. Machine learning-quantitative structure property  
385 relationship (ML-QSPR) method for fuel physicochemical properties prediction of  
386 multiple fuel types. *Fuel* 2021;304:121437.
- 387 [18] Wang H, Zhang B, Gong S, Wang L, Zhang X, Liu G. Experimental and modeling studies  
388 of quadricyclane and 2-ethylbornane pyrolysis from atmospheric to high pressure.  
389 *Combust Flame* 2021;226:163-181.
- 390 [19] Sirjean B, Herbinet O, Glaude PA, Ruiz-Lopez M, Fournet R. Theoretical Study of the  
391 Thermal Decomposition of a Jet Fuel Surrogate. *Proc. WSS/CI Spring 2008 Meeting*  
392 *Paper #08-S11*.
- 393 [20] Dagaut P, Cathonnet M, Rouan JP, Foulatier R, Quilgars A, Boettner JC, Gaillard F,  
394 James H. A jet-stirred reactor for kinetic studies of homogeneous gas-phase reactions at  
395 pressures up to ten atmospheres ( $\approx 1$  MPa). *J Phys E: Scientific Instruments*  
396 1986;19(3):207.
- 397 [21] Thion S, Togbé C, Serinyel Z, Dayma G, Dagaut P. A chemical kinetic study of the  
398 oxidation of dibutyl-ether in a jet-stirred reactor. *Combust Flame* 2017;185: 4-15.
- 399 [22] Thion S, Serinyel Z, Dayma G, Dagaut P. More insight into cyclohexanone oxidation:  
400 Jet-stirred reactor experiments and kinetic modeling. *Fuel* 2018;220: 908-915.
- 401 [23] Dayma G, Thion S, Serinyel Z, Dagaut P. Experimental and kinetic modeling study of  
402 the oxidation of cyclopentane and methylcyclopentane at atmospheric pressure. *Int J*  
403 *Chem Kinet* 2020;52(12): 943-956.
- 404 [24] RMG, <https://rmg.mit.edu/>; 2022 [accessed September 2022].

- 405 [25] M. J. Frisch, G. W. Trucks, H. B. Schlegel, et al., Gaussian, Inc., Wallingford CT, 2016.
- 406 [26] Krasnoukhov VS, Porfiriev DP, Zavershinskiy IP, Azyazov VN, Mebel AM. Kinetics of  
407 the CH<sub>3</sub> + C<sub>5</sub>H<sub>5</sub> Reaction: A Theoretical Study. The Journal of Physical Chemistry A  
408 2017;121(48):9191-9200.
- 409 [27] Hansen N, Kasper T, Yang B, Cool TA, Li W, Westmoreland PR, Oßwald P, Kohse-  
410 Höinghaus K. Fuel-structure dependence of benzene formation processes in premixed  
411 flames fueled by C<sub>6</sub>H<sub>12</sub> isomers. Proc. Combust. Inst. 2011;33(1):585-592.